RSC Advances

PAPER

View Article Online
View Journal | View Issue

Check for updates

Cite this: *RSC Adv.*, 2020, **10**, 20886

Preparation, characterization and evaluation of a new film based on chitosan, arginine and gold nanoparticle derivatives for wound-healing efficacy

Kai Wang, Zhiping Qi, Su Pan, Shuang Zheng, Haosheng Wang, YuXin Chang, Hongru Li, Pan Xue, Xiaoyu Yang* and Chuan Fu*

It is well-known that the combination of polymers and nanoparticles (NPs) provides optimised wound dressing and accelerates wound healing. The knowledge about the structure and properties of these materials is of critical importance in biological processes related to wound healing. In this study, we prepared a chitosan (CS) film modified with arginine (Arg) and gold NPs (AuNPs) and investigated its effectiveness as a dressing material for wound healing. Fourier-transform infrared spectroscopy (FTIR) confirmed that Arg was successfully grafted on CS. The resultant CS-Arg/AuNP film was then characterised by transmission electron microscopy (TEM) and scanning electron microscopy (SEM). The modification of Arg and AuNPs improved the hydrophilicity, mechanical strength and antibacterial properties of the film, which in turn provided an enhanced ideal environment for cell adhesion and proliferation. Cell Counting Kit-8 (CCK-8) was used to demonstrate the survival rate. Furthermore, the proteins involved in wound healing were evaluated qualitatively and quantitatively by immunofluorescence and western blotting, respectively. The skin defect models used for the *in vivo* studies revealed that the CS-Arg/AuNP dressing accelerated wound closure, re-epithelialization and collagen deposition. Our cumulative findings support the feasibility of using the proposed film as a promising candidate for tissue engineering of the skin in the near future.

Received 25th April 2020
Accepted 25th May 2020

DOI: 10.1039/d0ra03704d

rsc.li/rsc-advances

Open Access Article. Published on 02 June 2020. Downloaded on 1/17/2026 12:49:57 PM.
This article is licensed under a Creative Commons Attribution-NonCommercial 3.0 Unported Licence.

Introduction

Skin—the largest organ and the outermost layer of the human body—protects the body from external injuries, including numerous physical, chemical and microbial agents. Thus, skin defects after trauma remain a serious threat for the human body. Dermal transplantation is the mainstream treatment approach preferred by many patients. However, skin grafting procedures are limited by not only the scarcity of donors and the risks of immune rejection but also by the economic pressure on the patients. Cell therapy is another promising strategy for wound healing using cultured cell grafts, but the excessive time duration involved in acquiring adequate amounts of keratinocytes acts as another burden for the patients.[1]

In the recent years, wound dressing, as an appropriate strategy for tackling the above-mentioned issues, has been widely studied in the clinical medicine segment, especially in the field of surgery. Would healing is a complex physiological process that involves blood clotting, wound contraction, vascularization, inflammatory cytokine intervention, cell proliferation and finally fibrous connective tissue formation.[2] Ideal wound dressing materials should thus exhibit the following characteristics that are associated with promoted healing, including good biocompatibility, mechanical strength, water absorption, proliferation promotion, non-toxicity and antibacterial effects.[3] The new skin substitutes should ideally provide appropriate microenvironments for improving vascularization, reducing chemotaxis of inflammatory cytokines, enhancing cell proliferation and adhesion and eventually allowing progressive remodelling. Past studies have examined a variety of organic and inorganic materials in wound dressing alone and have achieved good outcomes.[4–6] Unfortunately, both these groups of materials have obvious disadvantages, mainly including poor mechanical properties of the organic materials and the weak biocompatibility of inorganic materials. Organic–inorganic nanocomposite materials can nevertheless integrate the advantages of the two materials and provide superior properties in terms of physical, chemical and biological properties; this option is currently being widely investigated.[5,7] It is thus important to identify suitable organic and inorganic candidates as dressing materials. In this view, polymers as an organic substance, such as gelatin, polyethylene glycol (PEG), chitin and chitosan (CS), are heralded as promising candidates based on their beneficial properties for wound healing.

Considering the origin of biopolymers, CS enjoys unique biocompatibility, biodegradability and non-toxicity, which is undoubtedly a merit in its application for wound healing.

The Second Hospital of Jilin University, Changchun, Jilin 130041, China. E-mail: yangxiaoy@jlu.edu.cn; fuchuan2015@163.com

This journal is © The Royal Society of Chemistry 2020

Open Access Article. Published on 02 June 2020. Downloaded on 1/17/2026 12:49:57 PM.
This article is licensed under a Creative Commons Attribution-NonCommercial 3.0 Unported Licence.

Several studies have demonstrated that CS is applicable in numerous fields related to tissue regeneration.[8–10] In addition, CS plays an active role in various stages of wound healing, such as in the cytokine production, macrophages activation and collagen synthesis, which together quicken the healing process. As a positively charged polymer,[11] it attracts growth factors and cytokines near the wound and promotes the deposition of type I collagen at the wound site. Structurally, CS gel has an appropriate porosity, which provides the required conditions to maintain the moisture and air permeability in a wound.[12] Although CS possesses numerous advantages, its application is restricted by its low mechanical strength and insufficient antibacterial properties. Considering these defects, a variety of modified CS alternatives has also been widely studied.[13,14]

The wounds are prone to infection, and infected wounds are characterised by progressively increasing volume of exudates, which inhibit the formation of granulation tissue, thereby delaying the healing process. CS has a relatively weak broad-spectrum antibacterial property owing to the positive charge carried by the amino groups, which interact with the negative charge on the bacterial surface, causing changes in the cell permeability as well as leakage of intracellular substances. Fortunately, this ability can be enhanced by increasing the number of positive charges, such as by grafting onto positively charged amino acids and loading with other antibacterial agents.[15–17] Arginine (Arg) is a typical positively charged amino acid. Once CS is modified by Arg, the enhancement of the positive ion group can attract more negatively charged cytokines and growth factors near the wound site and stimulate cell proliferation and differentiation there. Furthermore, Arg is a precursor of nitric oxide (NO) and an active molecule closely related to vascularization, immune response, epidermal cell proliferation and migration and late collagen deposition. Thus, this amino acid plays a significantly important role in wound healing.[18,19]

Recently, the use of nanoparticles (NPs) to enhance the physical and chemical properties of biopolymers has attracted the attention of scientists across the world. Among the inorganic materials mentioned earlier, gold NPs (AuNPs) stand out in virtue of their excellent antibacterial performances. Thus, AuNPs are the emerging candidates for repairing defects, especially in the skin.[20,21] Unlike other inorganic materials, AuNPs are chemically inert and size-tunable, and their processing can be controlled by different chemical synthesis methods, which in turn offer the option of changing their physical and chemical properties as desired. In addition, toxicity pertaining to Au is dramatically low when compared with other NPs like silver (Ag), iron oxide (Fe_3O_4) and zinc oxide (ZnO).[22] Moreover, the addition of AuNPs can increase the mechanical strength of CS matrix. The role of AuNPs is not only to protect the wound bed but also to act as a substitute space for the generation of tissues.[23] Finally, surface ligands of NPs can interact with polymer molecules in a multivalent manner to form self-therapeutic agents.[24] Under the coating of CS, the ligand structure of the NPs changes and they get surrounded by positive charges, which not only specifically destroy bacterial cell membranes but also inhibit the contact between planktonic bacteria and negatively charged cell surfaces through a strong electrostatic effect.

In the current work, an Arg and AuNPs-modified CS film was prepared as a synthetic material to provide improved wound dressing for skin repair. While exploring the effect of Arg grafting on AuNPs, this paper also explored whether the multivalent manner of AuNPs can offer full play to the advantages of Arg grafting. The chemical structure and morphology of the material under study were characterised by scanning electron microscopy (SEM), transmission electron microscopy (TEM) and Fourier-transformed infrared spectroscopy (FTIR). Next, the regenerative effect of the skin defects was evaluated by both *in vitro* and *in vivo* assays. This study, to the best of our knowledge, is the first-of-its-kind to investigate the effect of Arg and AuNPs-modified CS film on skin tissue engineering in a full skin damage condition.

Materials and methods

Materials

CS (deacetylation ≥ 95%; Aladdin, Shanghai, China), hydrogen tetrachloroaurate (III), $HAuCl_4 \cdot 3H_2O$ (Au ≥ 47.5%; Aladdin), NaOH (Sigma-Aldrich, St. Louis, MO, USA), acetic acid (Sigma-Aldrich), L-Arg (Aladdin), NHS (Aladdin), EDC (Aladdin), sodium citrate (Aladdin), Dulbecco's Modified Eagle's Medium (DMEM) and foetal bovine serum (Life Technologies, Carlsbad, CA, USA), trypsin (Solarbio, Beijing, China), methylthiazoletetrazolium (MTT; Gibco, Gaithersburg, MD, USA), trypsin, haematoxylin and eosin (H&E) and Masson trichrome staining kits (Solarbio) and Balb/c3T3 cells (National Centre for Cell Sciences, Pune, India).

Preparation of CS-L-Arg

Briefly, deacetylated CS (0.4 g) was dissolved in 20 mL of 1% (v/v) acetic acid with continuous stirring to achieve a final concentration of 2% (w/v) CS solution. Then, NHS and EDC were separately added to the CS solution and magnetically stirred until dissolved, followed by the supplementation of L-Arg to the solution. The resultant solution was dialysed for 3 days against distilled water. The final product was freeze-dried for 24 h and stored until further use.

Preparation of CS-AuNPs and CS-L-Arg/AuNPs

CS- and L-Arg-grafted CS were prepared as described in previous Section. $HAuCl_4 \cdot 3H_2O$ was then added at the same molar concentration as CS to distilled water at 75 °C for 30 min. Subsequently, sodium citrate was added to the mixture and the mixture was stirred well until a red-coloured solution appeared. Next, CS/AuNPs and CS-Arg/AuNPs were prepared by mixing gold gel solution in the CS and CS-Arg, respectively. The resulting solution was finally lyophilised to obtain a reserve powder.

Production of films

Three gels were obtained by dissolving CS and 2 other freeze-dried modified CS powders in distilled water and adding 1%

Open Access Article. Published on 02 June 2020. Downloaded on 1/17/2026 12:49:57 PM.
This article is licensed under a Creative Commons Attribution-NonCommercial 3.0 Unported Licence.

acetic acid to it. These gels were spread uniformly on the well and cross-linked with NaOH for 12 h. Next, the resultant material was disinfected under ultraviolet light for 12 h. Finally, all the materials prepared for the cell experiments were pre-processed in DMED medium for 6 h.

Chemical characterization by FTIR

The Arg coupling and chemical bonds and chemical groups were evaluated by FTIR (VERTEX 70; Bruker).

TEM

To better understand the size of AuNPs, TEM was performed. Briefly, the CS-Arg/Au solution was dropped onto a copper grid and the particle distribution was observed under the JEOL 2100 TEM at the room temperature.

SEM

For SEM analysis, 4 types of powder were sampled, including CS, CS-Arg, CS/Au and CS-Arg/Au. The ultrastructural morphology of the powder was observed under the Zeiss SEM, operated at 20 kV under high-vacuum conditions.

Mechanical properties

The universal mechanical testing machine (1121; Instron, UK) was used at a constant cross-head speed to detect the strain of 4 porous samples (30 mm) until the samples were thoroughly broken; at the same time, the values of tensile stress were recorded sequentially.

Hydrophilicity

The contact angle of 4 types of porous samples was measured by a contact angle apparatus (VCA 2000; AST) as the index of hydrophilicity. We fixed the samples and kept the surfaces flat. Next, 2 μL of double distilled water was carefully dripped onto the sample surfaces. Finally, the water droplets on the films were photographed and measured by docking the antennae.

Antibacterial activity

To evaluate the antibacterial activity of the films, antibacterial tests at OD 600 were performed against *Staphylococcus aureus* and *Escherichia coli*. Briefly, the materials were cut into 20 mm circles and sterilised under ultraviolet light for later use. Both the bacterial species (4.0×10^4 mL^{-1}) were cultured in lysogeny broth (LB) media for 2 h at 37 °C. Subsequently, 3 mL of the cultured bacteria were incubated with the sterilised material (0.5 g) for 10 h at 37 °C. Finally, the absorbances of the bacterial strains from each group were measured with a spectrophotometer at 600 nm to evaluate the antibacterial activities of the porous films.

Moreover, 5 mL of the bacterial suspension (4.0×10^4 mL^{-1}) was prepared in the LB medium. The 4 groups of sterilised materials (0.5 g) were respectively placed in a certain amount of suspension and cultured for 1 h at 37 °C. A fluorescent dye was then added to the suspension and incubated for 30 min. Finally, the bacterial viability was observed under a fluorescence microscope.

Cell proliferation experiment

CCK assays and immunofluorescence staining were performed to evaluate the effects of CS-Arg/AuNPs composites on the proliferation and adhesion of Balb/c3T3 cells. According to the different treatment methods employed, the experimental groups were divided into 4 groups: CS, CS/AuNPs, CS-Arg and CS-Arg/AuNPs.[25] Ten thousand cells were added to each well in a 64-well plate, and the survival and proliferation of each group of cells were evaluated by the CCK-8 when the cells adhered to the wall on days 1, 2 and 3. In order to better observe the morphology of cell growth in each group, the samples were observed under the fluorescence microscope.

Effects of materials on the protein levels

Immunofluorescence and immunoblotting analyses were conducted to quantitatively analyse the effects of materials on the expression of collagen I associated with wound healing in cells. Cell grouping and material processing were performed as described earlier. After 3 days of culturing, for immunofluorescence, the medium was removed and the cells were fixed with 4% paraformaldehyde for 15 min and then washed with PBS thrice, each time for 5 min. The cells were then left to rest at the room temperature for 30 min. The cells were treated with collagen I primary antibody and placed in a wet box for 4 nights. Next, the cells were washed thrice with phosphate-buffered saline (PBS), incubated with a specific secondary antibody at the room temperature for 2 h and washed thrice again with PBS. Finally, the samples were successively processed in 4′,6-diamidino-2-phenylindole (DAPI), washed thrice and then observed under the fluorescence microscope.

Next, western blotting experiments were performed. Briefly, the proteins in the cells were extracted using lyses buffer. After the centrifugation step, the proteins were quantified by the BCA Protein Assay Kit, normalised to a uniform concentration by adding the extraction buffer and denatured at 100 °C for 5 min. Next, the proteins from each cell group were run through 10% sodium dodecyl sulfate-polyacrylamide gel electrophoresis at 125 V and transferred on to a nitrocellulose membrane at 90 V. The membranes were then blocked with 5% non-fat dried milk at 37 °C for 1 h and incubated with the following primary antibodies at 4 °C: anti-collagen I (rat), anti-VEGF (rat) and anti-β-actin (rat). After overnight incubation with the antibodies, the membranes were washed thrice with Tris-buffered saline–Tween 20 (TBS–T) and further incubated with horseradish peroxidase (HRP)-conjugated secondary antibodies (rat). Finally, the proteins were visualised using enhanced chemiluminescence (ECL) detection reagents.

In vivo wound healing assessment

Adult male Sprague-Dawley rats ($n = 20$, wight: 250 g) were used to evaluate the status of wound healing. The animals were bred in a standard animal room by the same breeder, with filtered water and pellet food readily available. The animals were randomly allocated into 4 groups: Cs, CS/AuNPs, Arg-Cs and Arg-CS/AuNPs ($n = 5$ per group).[18,26] Each rat was numbered on

 This journal is © The Royal Society of Chemistry 2020

Open Access Article. Published on 02 June 2020. Downloaded on 1/17/2026 12:49:57 PM.
This article is licensed under a Creative Commons Attribution-NonCommercial 3.0 Unported Licence.

the tail and raised in different cages. All experimental protocols were approved by the Animal Care and Use Committee of the Jilin University, China and were conducted in accordance with the Guide for the Care and Use of Laboratory Animals of Jilin University and approved by the Animal Ethics Committee of Jilin University. The rats were anesthetised with intraperitoneally injected chloral hydrate. Two days before the experiment, the back hair of the rats was removed using a depilating cream. Four different films were soaked in alcohol for 24 h to be sterilised under ultraviolet light. After the rats were anaesthetised, they were placed in the prone position such that their back skins were fully exposed and then disinfected using iodine. Using a pre-prepared plastic mould, a full-thickness skin defect of 1.5 cm diameter was created on the back and photographed. Each skin defect was covered with a corresponding film, wrapped with sterile cotton surgical gauzes and fixed with breathable bandage. In order to avoid adhesion and contamination, the wound dressings were changed every 3 days after surgery and photographed. The wound healing rates were measured and evaluated by image analysis software (Image J). The healing rate was calculated according to the following formula: wound healing rate $= [(S_0 - S_n)/S_0] \times 100\%$, where S_0 is the initial size of the wound and S_n is the size of the wound at each observation point.

Histopathological staining

For histological examination of each group, all rats were euthanised on the 12th day of the surgery. The wound and the surrounding skin were completely removed for histopathological staining. The specimens for histopathological staining were fixed with formalin, dehydrated with alcohol, cleared with xylene, embedded in paraffin, and then sectioned vertically into 5 μm thick sections. After staining with H&E and Masson, histological changes were observed under an optical microscope.

Statistical analysis

Data were analysed using the Origin 8.0 software (Origin Lab; Los Angeles, CA, USA). Statistical differences between the data were assessed with one-way analysis of variance and *post hoc* test. Data were expressed as the mean ± standard. Final results with $P < 0.05$ were considered statistically significant.

Results and discussion

As shown in Fig. 1, the films were prepared and their effects on wound healing were explored through cell experiments, bacteriostatic experiments and *in vivo* animal experiments.

FTIR

The successful grafting of Arg onto CS *via* EDC/NHS coupling chemistry was detected by FTIR. Fig. 2 shows the FTIR spectra of CS and CS-Arg. The peak at 3435 cm^{-1} was assigned to the characteristic –NH and –OH stretching vibration. Peak near the 1414 cm^{-1} was assigned to the bending vibration of the single-bond C–H group. In addition, the characteristic peaks present at 1647 and 1563 cm^{-1} were assigned to the amide I and II bands, respectively. Arg exhibits an absorption band at 1628 cm^{-1} that was assigned to the guanidine group. The peaks found at 3299 and 3358 cm^{-1} belong to the stretching vibration peak of $-NH_2$, and the peak of 1679 cm^{-1} is the stretching vibration peak of carboxy carbonyl group. In the FTIR spectra of CH-Arg (Fig. 2A), the peak at 3441 cm^{-1} was assigned to the stretching vibration of –NH and –OH, and the peak strength was reduced, which indicates that the content of hydroxyl and amino groups was reduced after modification. Furthermore, the peak at 1064 cm^{-1} was attributed to the stretching vibration peak of C–O, which suggests that Arg is indeed linked to the CS backbone.[18,27]

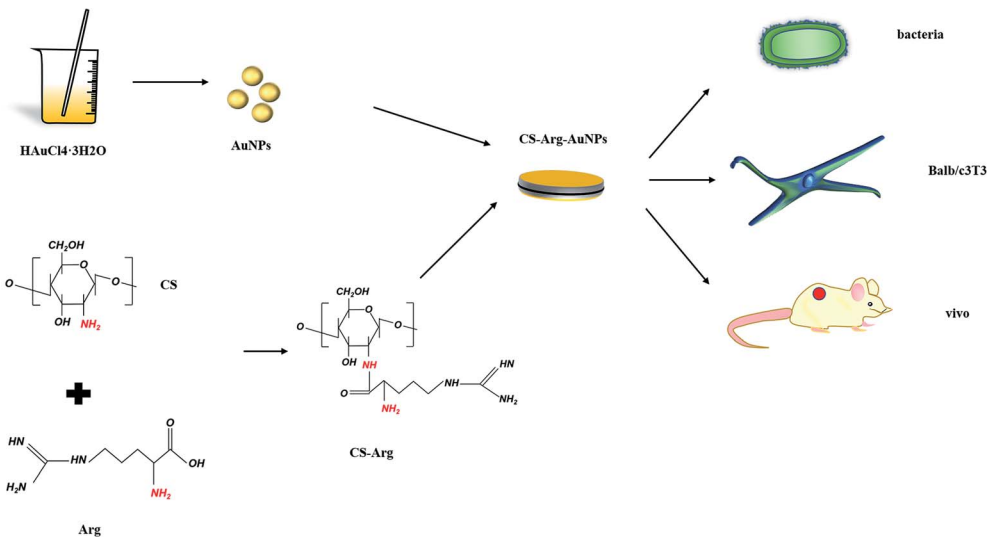

Fig. 1 The flow chart depicting the study protocol. Cs-Arg/AuNPs was prepared in the form of film. Next, the wound-healing efficacy and bacteriostatic effect were investigated through *in vitro* bacterial, Balb/c3T3 cell and *vivo* animal experiments.

Open Access Article. Published on 02 June 2020. Downloaded on 1/17/2026 12:49:57 PM.
This article is licensed under a Creative Commons Attribution-NonCommercial 3.0 Unported Licence.

TEM

Fig. 3A shows the highly magnified TEM image of AuNPs. The particle size and distribution were determined using the image analysis software (Image J). According to the statistical evaluation, most of the prepared AuNPs were spherical and dispersed with an average size of 10 nm (Fig. 2B and C). Although the toxicity of AuNPs is significantly lower than that of other metal NPs, size-dependent toxicity has been reported for AuNPs. Recent studies have reported that AuNPs of particle size < 2 nm exhibited higher toxicity as compared to the larger ones.[28,29] In addition, spherical AuNPs of size 10–20 nm exhibited less cytotoxicity and more bacteriostatic properties. Chitosan with a medium molecular weight acts as a better stabilizing agent,[30] which may be related to the size distribution of AuNPs; however, the specific mechanisms in this event remain unclear.

SEM

The microstructure and roughness of the film play important roles in cellular attachment, migration and proliferation in tissue engineering. SEM images of the surfaces of CS, CS-Arg, CS/AuNPs and CS-Arg/AuNPs are shown in Fig. 2D. The results revealed that the graft of Arg and the modification of AuNPs increased the roughness of the CS film surface. In particular, some large AuNPs were observed in Au-Cs and Arg-Au-Cs. As reported in previous studies, a certain degree of roughness not only improves the cell affinity but also increases the contact area with the wound and thereby accelerates the haemostatic process.[31–33] Therefore, change in the morphology of CS as well as its improved biocompatibility may be due to the modification of Arg and AuNPs.

Mechanical properties

The composite material must have sufficient mechanical strength to better adapt to the changes in the wound surface morphology and structure during the healing process. In addition, prior studies have reported that the superior mechanical strength is beneficial not only for cell adhesion but also for wound shaping to accelerate wound recovery.[34] The poor mechanical strength of CS is an important factor that restricts its wide applications in wound healing.[35] However, the graft of Arg and the addition of AuNPs can significantly improve

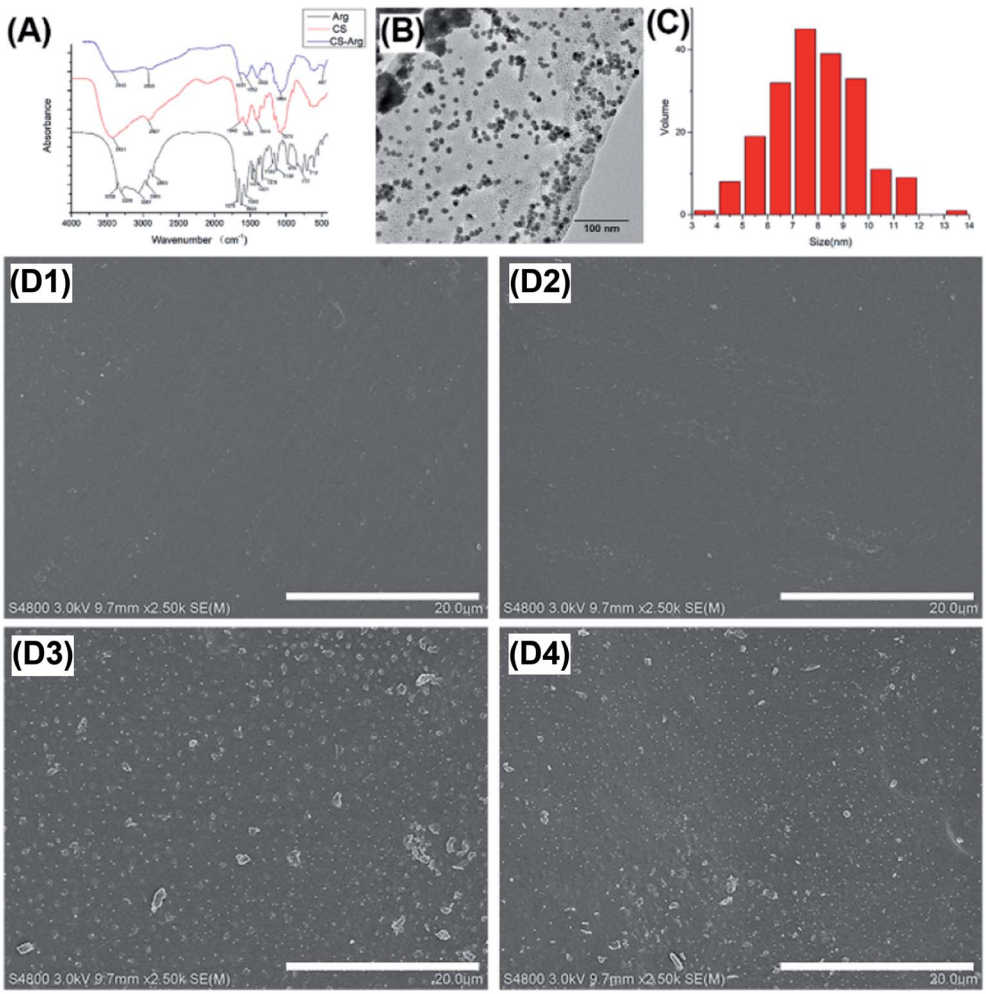

Fig. 2 FTIR spectra of CS, Arg and CS-Arg (A), TEM of CS-Arg/AuNPs (B), the size distribution of CS-Arg/AuNPs (C), SEM images of the surfaces of the CS (D1), CS-Arg (D2), CS/AuNPs (D3) and CS-Arg/AuNPs (D4).

 This journal is © The Royal Society of Chemistry 2020

Open Access Article. Published on 02 June 2020. Downloaded on 1/17/2026 12:49:57 PM.
This article is licensed under a Creative Commons Attribution-NonCommercial 3.0 Unported Licence.

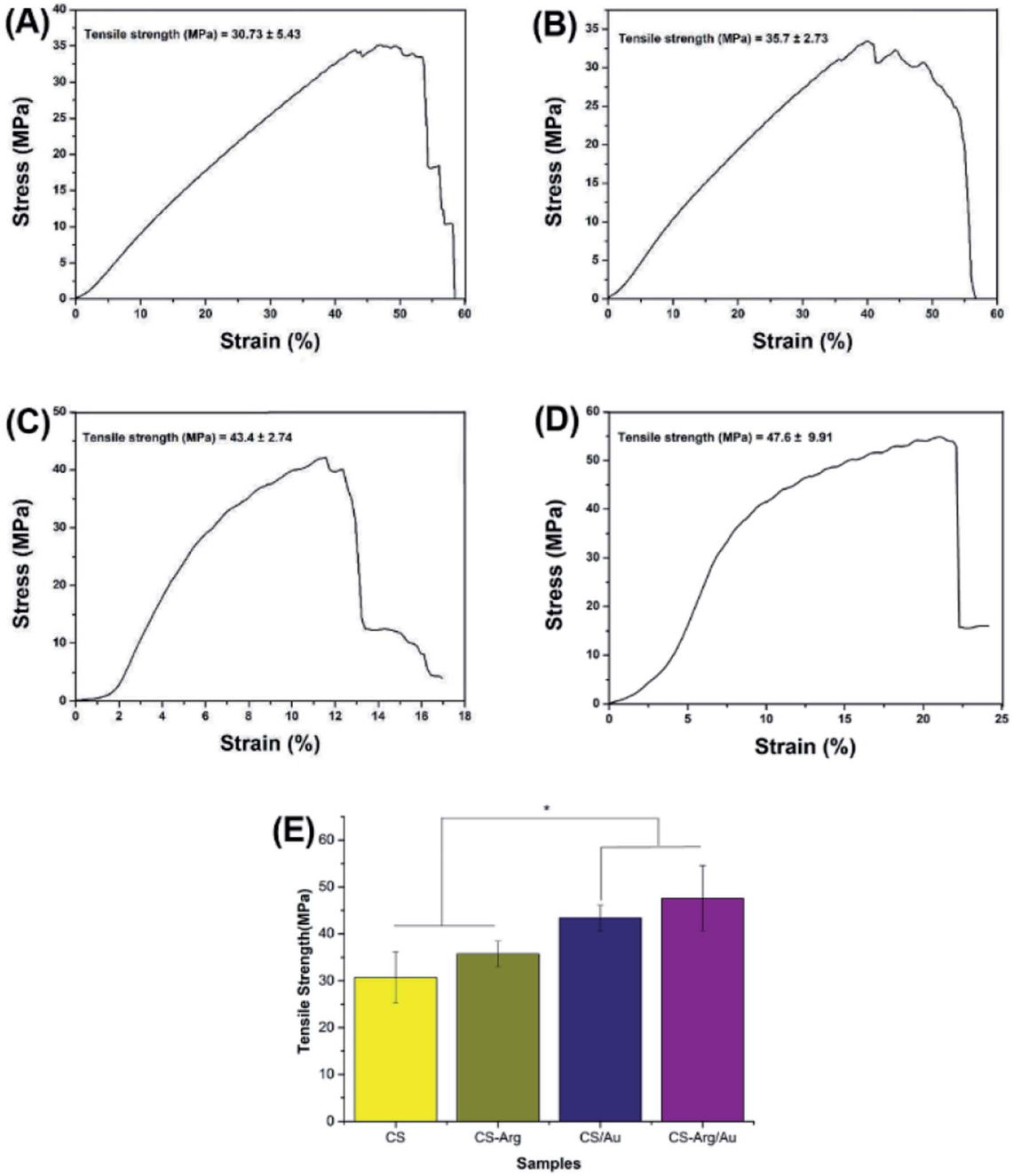

Fig. 3 Tensile strength of the CS (A), CS-Arg (B), CS/AuNPs (C) and CS-Arg/AuNPs (D). The measured tensile strength (E). Error bars represent the mean ± SD ($n = 3$; * denotes statistically significant difference *$p < 0.05$).

the mechanical strength of CS. Fig. 3 gives the tensile strength of different films. The $-NH_2$ group of Arg combines with the –COOH group of CS to form an amide bond, this intramolecular force may account for the better tensile strength of Arg-modified CS in comparison with that of CS alone. The addition of AuNPs also significantly improved the tensile strength of CS. Based on previous reports, the use of AuNPs of appropriate size and dispersion can help improve the overall mechanical strength of the resultant nanocomposites.[36,37] Meanwhile, some studies suggest that intermolecular interactions between AuNPs and CS may also contribute to the improvement of the mechanical strength of the final product.[38]

Hydrophilicity

Hydrophilicity is another surface property of a material that affects its healing efficiency. Previous studies have shown that a hydrophilic surface is conducive to the adsorption of serum proteins, which is an important prerequisite for cell adhesion and proliferation.[39–41] Fig. 4 shows the contact angles of different films, which is the indicator of hydrophilicity. As can be seen in the figure, the hydrophilicity of CS was enhanced by

Open Access Article. Published on 02 June 2020. Downloaded on 1/17/2026 12:49:57 PM.
This article is licensed under a Creative Commons Attribution-NonCommercial 3.0 Unported Licence.

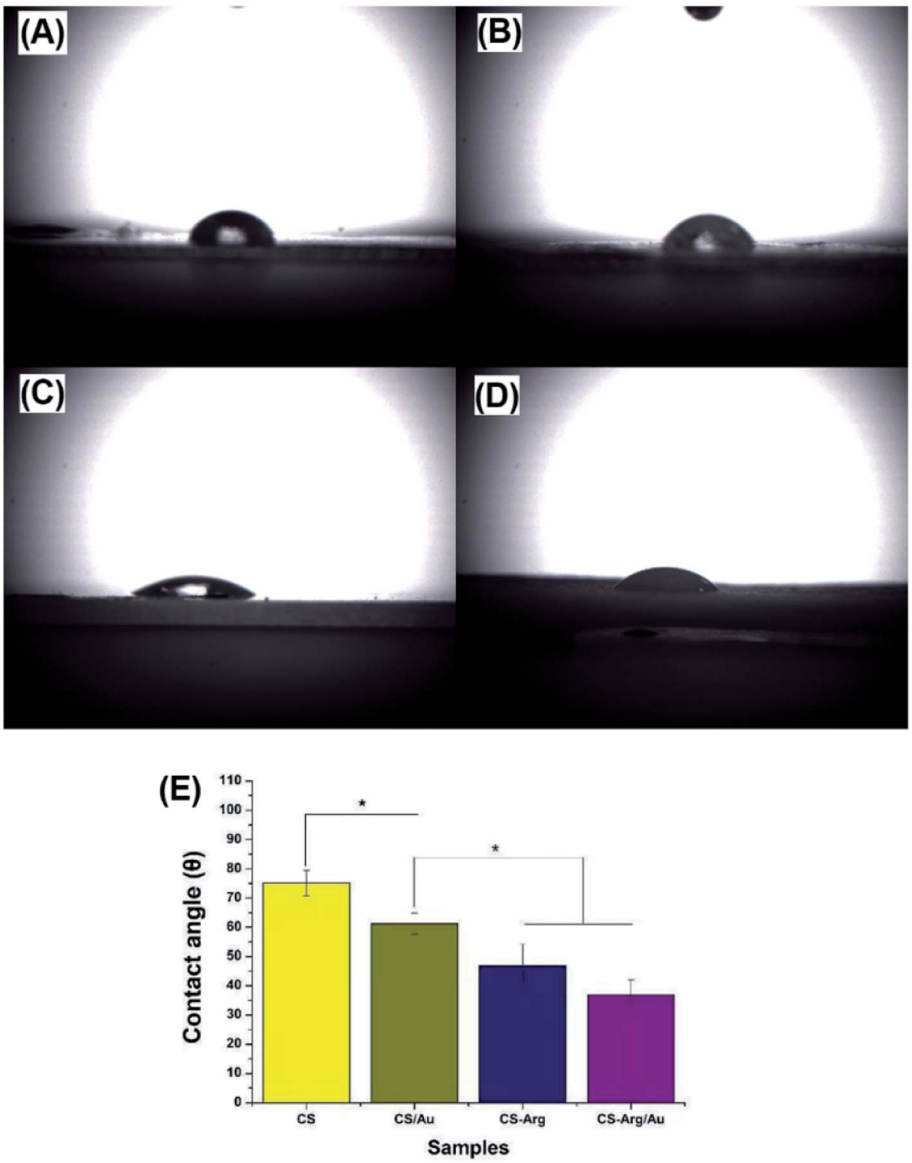

Fig. 4 Contact angles of the CS (A), CS-AuNPs (B), CS-Arg (C) and CS-Arg/AuNPs (D). The measured contact angle (E). Error bars represent the mean ± SD ($n = 3$; * denotes statistically significant difference *$p < 0.05$).

the modification of Arg and AuNPs. The improved hydrophilicity of CS-Arg can be attributed to the presence of hydrophilic groups, including –OH, –NH_2 and –COOH. The addition of AuNPs also improved the hydrophilicity of the composites, and this phenomenon can be likely attributed to the fact that AuNPs reduced the steric effect of cross-linking and resulted in high surface homogeneity.[42] In addition, according to a previous study, Arg and AuNPs can effectively change the surface morphology of CS, and a rough surface can host and disperse more fluids—these points may offer further explanation for the improved hydrophilicity of the material.[43] Therefore, as compared with CS alone, CS-Arg/AuNPs can provide a more suitable microenvironment for cell adhesion and proliferation.

Antibacterial activity

Without the integrity, the skin loses its natural barrier against bacteria. Simultaneously, exudate from necrotic tissues can cause bacterial infections, which delay the wound healing process. Therefore, excellent bacteriostatic properties are essential in an ideal dressing material. CS, as a natural cationic polymer, combines with anionic phospholipids on the surface of the bacterial cell *via* charge effect to achieve antibacterial properties. However, these properties have been reported to have several limitations.[44,45] The graft of Arg can enhance the positive charge of CS and generate the bacteriostatic effect through the charge effect. Furthermore, AuNPs exert antibacterial properties against Gram-negative and Gram-positive bacteria without causing drug resistance. According to most

 This journal is © The Royal Society of Chemistry 2020

Open Access Article. Published on 02 June 2020. Downloaded on 1/17/2026 12:49:57 PM.
This article is licensed under a Creative Commons Attribution-NonCommercial 3.0 Unported Licence.

past studies, this mechanism can be attributed mainly to the ability of AuNPs to block the electrostatic flux between the membranes, creating a distortion in the membrane and ultimately in a break-down.[46] Moreover, while killing bacteria, AuNPs produce reactive oxygen species (ROS) that continually destroy the pathogen's cellular components.

The antibacterial properties of the modified CS were evaluated by OD 600 antibacterial tests against *S. aureus* and *E. coli*. As shown in Fig. 5, lower optical density was recorded in the bacterial suspension co-cultured with the CS-Arg/AuNPs film as compared with the suspension co-cultured with other films. Thus, the antibacterial properties of CS were significantly improved by the modification of Arg and AuNPs, especially by the latter. In addition, the OD value of the suspension was higher against *S. aureus* than against *E. coli*; this finding is consistent with the reports from previous studies.

In addition, the live/dead assay was performed to further confirm the antibacterial effect of the modified CS. Under the fluorescence microscope, bacteria with intact cell membranes appeared green, while the dead ones appeared red. The red signals increased significantly in the CS-Arg and CS/AuNPs groups as compared with that in the CS group; almost no green signals were recorded in the Arg-CS/AuNPs group (Fig. 6).

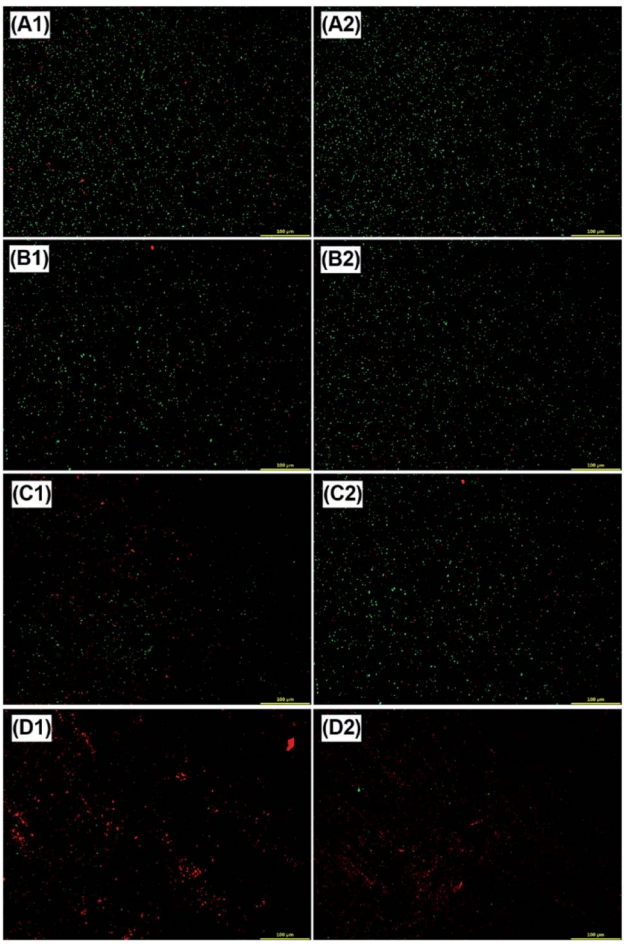

Fig. 6 Live/dead bacteria staining of CS (A), CS-Arg (B), CS/AuNPs (C) and CS-Arg/AuNPs (D) against *E. coli* (1) and *S. aureus* (2), scale bar: 100 μm.

Cell proliferation experiment

Balb/c3T3 cells are routinely applied, owing to their important role, in the studies of wound repair, including that in the release of growth factors and the formation of myofibroblasts to retract the wound. To observe the effects of modified CS on cell survival, the Cell Counting Kit-8 (CCK-8) assays were performed on days 1, 2 and 3; the results of the assays are presented in Fig. 7. Although the presence of CS can reduce the cytotoxicity of AuNPs to some extent,[47] several studies have shown that the cytotoxicity of AuNPs is dose-dependent. Therefore, based on the results of previous experiments, we selected AuNPs at a concentration of 120 ppm.[46,48] On the culture day 1, no statistically significant differences were noted among the groups. On culture day 3, however, the number of fibroblasts increased significantly in both the groups, CS-Arg and CS-Arg/AuNPs. On culture day 7, fibroblast survival continued to increase in the other experimental groups when compared with that in the CS and CS/AuNPs groups, the latter was particularly low for the toxicity of AuNPs.

Based on the experimental results, on one hand, although AuNPs exhibited antioxidative effects by effectively quenching

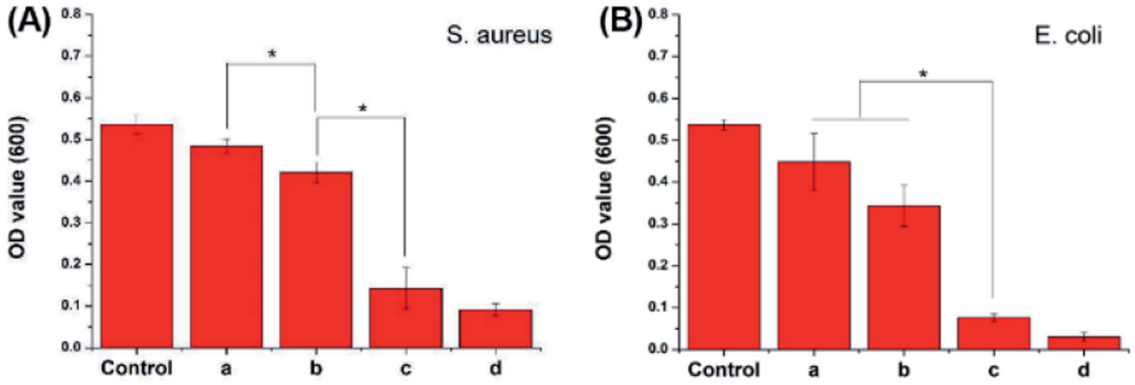

Fig. 5 Average OD at 600 nm (OD 600) of CS (a), CS-Arg (b), CS/AuNPs (c) and CS-Arg/AuNPs (d) against *S. aureus* (A) and *E. coli* (B). Error bars represent the mean ± SD ($n = 3$; * denotes statistically significant difference, $*p < 0.05$).

Open Access Article. Published on 02 June 2020. Downloaded on 1/17/2026 12:49:57 PM.
This article is licensed under a Creative Commons Attribution-NonCommercial 3.0 Unported Licence.

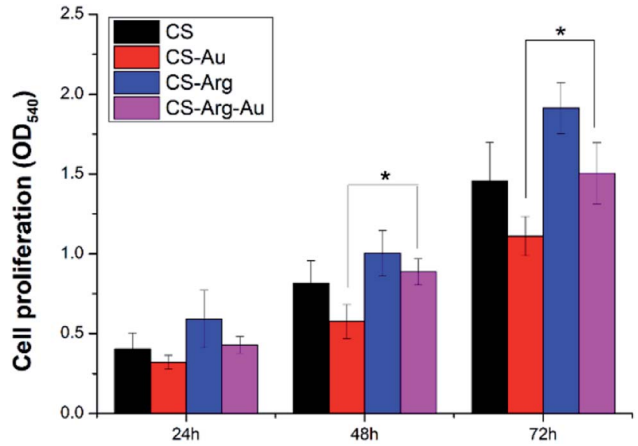

Fig. 7 The CCK-8 assays of Balb/c3T3 cells cultured on CS, CS/AuNPs, CS-Arg and CS-Arg/AuNPs. Error bars represent the mean ± SD ($n = 3$; * denotes statistically significant difference *$p < 0.05$).

the free radicals like 2,2-diphenyl-*l*-picrylhydrazyl (DPPH), OH (hydroxyl), H_2O_2 (hydrogen peroxide), and NO, thereby repairing damaged collagen tissues and reducing cell death, which indicated some degree of cytotoxicity. On the other, cytotoxicity could be significantly decreased in the presence of CS and CS-Arg. The improved cell compatibility of CS/AuNPs may be due to the coating of CS, which alleviates the cytotoxicity of AuNPs.[47] In addition, the modification of Arg significantly improved the cellular affinity of CS, which can be explained by the charge effect. Moreover, the changes in the surface morphology and hydrophilicity also improved the cell adhesion and proliferation abilities of the materials.

Effects of materials on protein levels

Fibroblasts achieved epidermal remodelling and vascularization by regulating the expression of related proteins, including collagen I and VEGF. During the wound healing process, fibroblasts gradually secreted increasing amount of collagen I, which in turn provided suitable conditions for the proliferation of fibroblasts and epidermal cells, and VEGF promoted the growth of vascular endothelial cells, thereby improving the hypoxic environment of the extracellular matrix (ECM).[49] First, we performed immunofluorescence staining to qualitatively observe the change in collagen I in each group. As shown in Fig. 10, the expression levels of collagen I in the CS-Arg and CS-Arg-AuNPs groups were significantly higher than those in the pure CS group; this observation is consistent with the results of a previous study.[50] In addition, we found that fibroblasts in CS-Arg and CS-Arg-AuNPs groups had better cytoskeleton and stretch activity relative to that in the CS group, which was also consistent with the results of MTT assays. Therefore, these 2 modification methods are expected to have positive effects on the expression of the related proteins.

Furthermore, western blotting was performed in order to quantitatively observe the expression of collagen I and VEGF in different intervention groups. As shown in Fig. 8, the trend of WB bands confirmed the results of immunofluorescence staining, indicating that the Au-CS-Arg group was the most effective one in promoting proteins related to tissue repair. However, the exact mechanism remains unclear. We therefore propose that the positive functions at the protein level are inseparable from the pro-proliferative effect of Arg.

In vivo wound healing assessment

To demonstrate their practical applicability, composites were used as wound dressing materials. As shown in Fig. 9, the general macroscopic photographs of postoperative wound healing at different time points after wounding were observed and calculated to evaluate the degree of wound contraction among the groups. All the wounds showed inflammatory response, while the CS group showed infection and mild oedema; however, no statistical difference was noted in the degree of contraction among the groups on day 3. The wound contraction ratio in the CS, CS/AuNPs, CS-Arg and CS-Arg/AuNPs groups increased in this order, gradually, until the sacrifice on day 12. On day 12, complete re-epithelialization of the wound was noted in the CS-Arg-Au group, while the wounds in the other groups failed to heal completely. The macroscopic appearance and the percent of contraction indicated that the CS-Arg/AuNPs composite greatly accelerated wound healing when compared with the CS, CS-Arg and CS/AuNPs. These excellent characteristics of CS-Arg-Au may be attributed to its remarkable antibacterial property, hydrophilic nature, mechanical strength and biocompatibility.

Histological assessment

The outcomes of wounds and the surrounding tissues shown in Fig. 10 using H&E staining and Masson's trichrome (MT) staining exhibited the histological features of each specimen (CS, CS-Arg, CS-Au and CS-Arg-Au). HE staining showed that the wound size remained large, accompanied by a thin regenerated epithelium and a clearly demarcated subepidermal space in the CS and CS-Au groups. In addition, the tissue defects were surrounded by significant inflammatory cells infiltration in the CS group, but only fewer inflammatory cells in the CS-Au and CS-Arg-Au groups. This phenomenon explained that AuNPs exhibited anti-inflammatory properties, as also proved by past studies.[51] On the contrary, vascularised granulated tissues covered with a thin, uniform and complete epidermis could be observed in the CS-Arg and CS-Arg-Au groups, especially in the latter, while only slight granulation was observed in the CS and CS-Au groups, suggesting that CS-Arg/AuNPs can accelerate the proliferation of fibroblast and angiogenesis capabilities. At the healing stage, the thickness of the re-epithelialization thickened first and then gradually thinned until it returned to normal thickness. In addition, new-born hair follicles were observed in the CS-Arg/AuNPs group. The granulation tissue included newly forming blood vessels and collagen fibres. Therefore, MT staining was performed for the examination of collagen fibres.

Fibroblast synthesised collagen fibres is known to form the ECM. Furthermore, the deposition of ECM in turn promotes fibrosis formation by providing the substrate for fibroblast

 This journal is © The Royal Society of Chemistry 2020

Open Access Article. Published on 02 June 2020. Downloaded on 1/17/2026 12:49:57 PM.
This article is licensed under a Creative Commons Attribution-NonCommercial 3.0 Unported Licence.

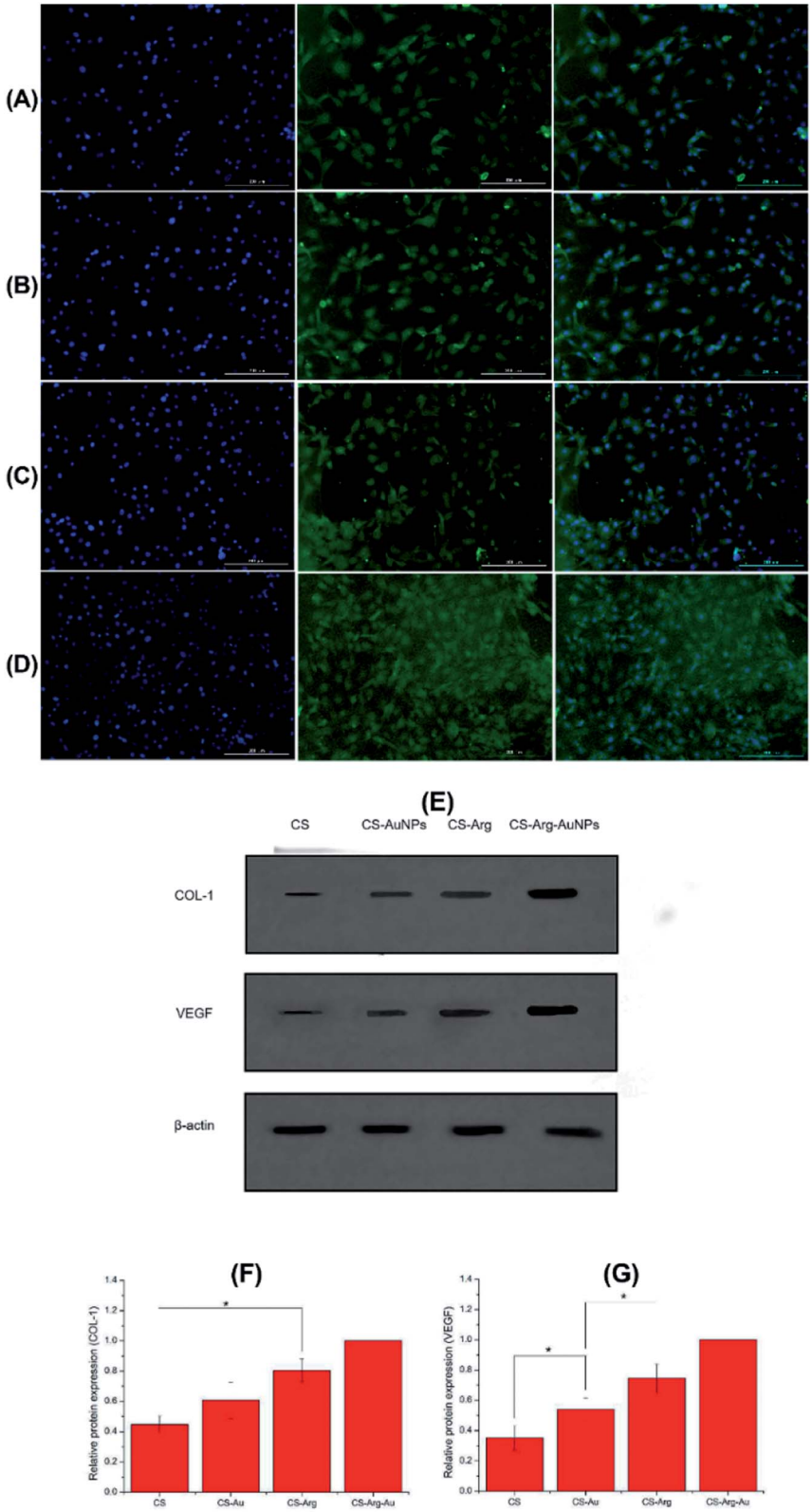

Fig. 8 Immunofluorescence images of COL-1 protein under different culture conditions. CS (A), CS/AuNPs (B), CS-Arg (C) and CS-Arg/AuNPs (D). Scale bars = 200 μm. The specific band of protein (COL-1, VEGF and β-actin) of each group tested by western blotting (E). The relative intensity of the bands from each group (CS, CS/AuNPs, CS-Arg and CS-Arg/AuNPs) ((F) COL-1; (G) VEGF).

Open Access Article. Published on 02 June 2020. Downloaded on 1/17/2026 12:49:57 PM.
This article is licensed under a Creative Commons Attribution-NonCommercial 3.0 Unported Licence.

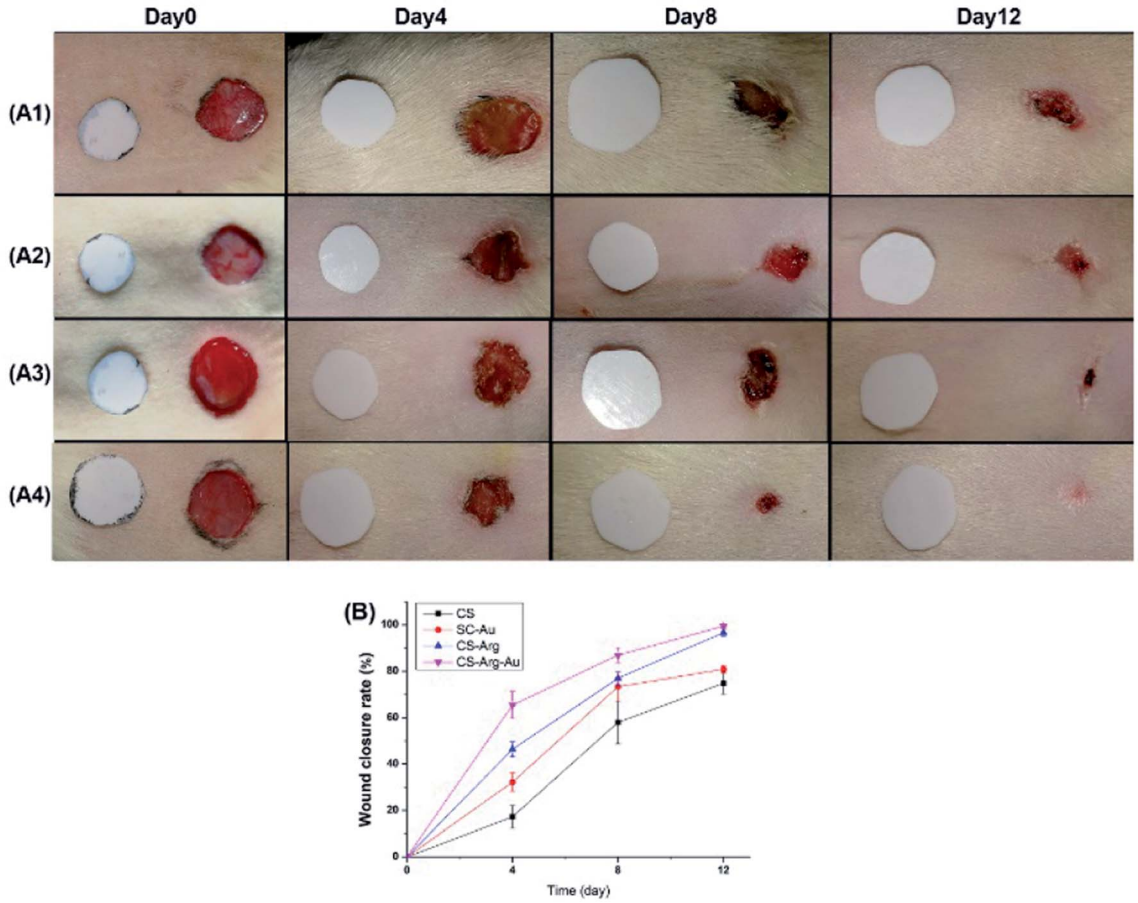

Fig. 9 The differential effects of composites on wound healing. (A) Representative macroscopic appearance of wounds. CS (A1), CS/AuNPs (A2), CS-Arg (A3) and CS-Arg/AuNPs (A4). Wound-healing curves (B). * Error bars represent the mean ± SD ($n = 3$; * denotes statistically significant difference *$p < 0.05$).

adhesion. Hence, collagen fibres play a crucial role in the process of wound healing. When compared with those in the CS-Arg and CS-Arg-Au groups, collagen fibres in the CS and CS-Au groups were disorganised and fragmented, which may be because Arg effectively stimulates collagen fibres released from fibroblasts.[52,53] Untidy and loose collagen fibres were observed in the CS and CS-Au groups, while well-organised collagen fibres were observed in the CS-Arg and CS-Arg/AuNPs groups. In addition, the CS-Au group displayed higher expression of collagen fibres than the CS group, which may be attributed to

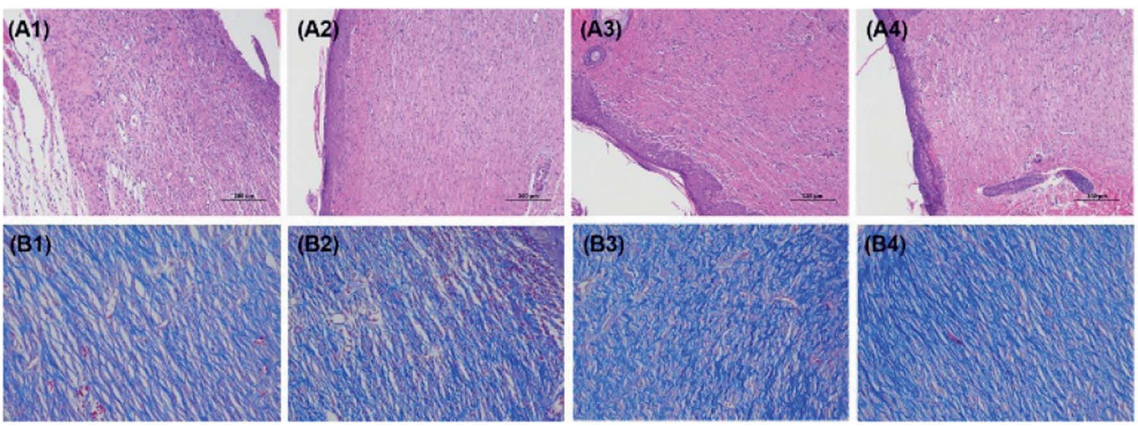

Fig. 10 Differential effects of composites on the histological features of wounds at day 12. (A) H&E staining, scale bar: 200 μm (B) MT staining, scale bar: 100 μm of CS (1), CS/AuNPs (2), CS-Arg (3) and CS-Arg/AuNPs (4).

 This journal is © The Royal Society of Chemistry 2020

Open Access Article. Published on 02 June 2020. Downloaded on 1/17/2026 12:49:57 PM.
This article is licensed under a Creative Commons Attribution-NonCommercial 3.0 Unported Licence.

the antibacterial properties of AuNPs. These results suggest that the CS-Arg/AuNPs treated wound tissues have a considerable amount of collagen deposition and tightly arranged fibre network.

Conclusions

In this study, CS-Arg/AuNPs films were synthesised by modification of CS with Arg and AuNPs; the efficiency of the films were characterised by FTIR, TEM and SEM. Based on the physical and chemical analyses, the resultant composites were found to exhibit excellent mechanical properties, hydrophilicities and antibacterial activities owing to the presence of chemical bond and metal NPs. In addition, CS-Arg-Au showed a rougher surface compared to the other groups, which was conducive for fibroblasts to adhere, proliferate and secrete proteins associated with tissue repair mechanisms. Moreover, a series of further *in vivo* experiments demonstrated that CS-Arg/AuNPs showed a faster speed of wound contraction as well as exhibited a thin layer of re-epithelialization, dense collagen deposition and clearly visible neovascularization in the histological analysis. Overall, our work demonstrated that CS-Arg/AuNPs film can prevent further infection of a wound to a large extent and reduce the healing time. Therefore, it has potential utility across the field of wound healing medication and interventions.

Conflicts of interest

There are no conflicts to declare.

Acknowledgements

The study was supported by the Changchun Science and Technology Plan Project (No. 18YJ012).

References

1 C. C. Yates, D. L. Whaley and A. Wells, Deficient Dermal Remodeling Corrected by Adult and Fetal Fibroblasts Transplantation, *Wound Repair Regen.*, 2011, **19**, A61.

2 S. Ghanaati, P. Booms, A. Orlowska, A. Kubesch, J. Lorenz, J. Rutkowski, C. Landes, R. Sader, C. J. Kirkpatrick and J. Choukroun, Advanced Platelet-Rich Fibrin: A New Concept for Cell-Based Tissue Engineering by Means of Inflammatory Cells, *J Oral Implantol.*, 2014, **40**, 679–689.

3 P. Zarrintaj, A. S. Moghaddam, S. Manouchehri, Z. Atoufi, A. Amiri, M. A. Amirkhani, M. A. Nilforoushzadeh, M. R. Saeb, M. R. Hamblin and M. Mozafari, Can regenerative medicine and nanotechnology combine to heal wounds? The search for the ideal wound dressing, *Nanomedicine*, 2017, **12**, 2403–2422.

4 B. Dalisson and J. Barralet, Bioinorganics and Wound Healing, *Adv. Healthcare Mater.*, 2019, **8**(18), 1900764.

5 A. Jafari, S. Hassanajili, M. B. Karimi, A. Emami, F. Ghaffari and N. Azarpira, Effect of organic/inorganic nanoparticles on performance of polyurethane nanocomposites for potential wound dressing applications, *J. Mech. Behav. Biomed. Mater.*, 2018, **88**, 395–405.

6 C. Stewart, S. Parkins and K. LaiHing, Synergestic effects of organic nanofibers, honey and antibiotics for wound dressings, *Abstr. Pap. Am. Chem. Soc.*, 2018, **255**, 1282.

7 J. A. Oshiro, L. M. Shiota and L. A. Chiavacci, Development of organic-inorganic polymeric film formers for controlled drug release and wound care, *Materia-Brazil*, 2014, **19**, 24–32.

8 M. Lotfi, H. Naderi-Meshkin, E. Mandipour, A. Mafinezhad, R. Bagherzadeh, H. R. Sadeghnia, H. Esmaily, M. Maleki, H. Hasssanzadeh, M. Ghayaour-Mobarhan, *et al.*, Adipose tissue-derived mesenchymal stem cells and keratinocytes co-culture on gelatin/chitosan/beta-glycerol phosphate nanoscaffold in skin regeneration, *Cell Biol. Int.*, 2019, **43**, 1365–1378.

9 J. H. Shao, Z. R. Ding, L. X. Li, Y. Chen, J. Zhu and Q. R. Qian, Improved accumulation of TGF-beta by photopolymerized chitosan/silk protein bio-hydrogel matrix to improve differentiations of mesenchymal stem cells in articular cartilage tissue regeneration, *J. Photochem. Photobiol., B*, 2020, **203**, 111744.

10 J. Z. Si, Y. H. Yang, X. L. Xing, F. Yang and P. Y. Shan, Controlled degradable chitosan/collagen composite scaffolds for application in nerve tissue regeneration, *Polym. Degrad. Stab.*, 2019, **166**, 73–85.

11 Y. T. He, J. Miao, S. Q. Chen, R. Zhang, L. Zhang, H. L. Tang and H. Yang, Preparation and characterization of a novel positively charged composite hollow fiber nanofiltration membrane based on chitosan lactate, *RSC Adv.*, 2019, **9**, 4361–4369.

12 C. B. Dai, Y. Li, W. Z. Pan, G. Q. Wang, R. Q. Huang, Y. Y. Bu, X. J. Liao, K. J. Guo and F. L. Gao, Three-Dimensional High-Porosity Chitosan/Honeycomb Porous Carbon/Hydroxyapatite Scaffold with Enhanced Osteoinductivity for Bone Regeneration, *ACS Biomater. Sci. Eng.*, 2020, **6**, 575–586.

13 M. S. de Luna, C. Ascione, C. Santillo, L. Verdolotti, M. Lavorgna, G. G. Buonocore, R. Castaldo, G. Filippone, H. Xia and L. Ambrosio, Optimization of dye adsorption capacity and mechanical strength of chitosan aerogels through crosslinking strategy and graphene oxide addition, *Carbohydr. Polym.*, 2019, **211**, 195–203.

14 F. Dong and S. J. Li, Wound Dressings Based on Chitosan-Dialdehyde Cellulose Nanocrystals-Silver Nanoparticles: Mechanical Strength, Antibacterial Activity and Cytotoxicity, *Polymers*, 2018, **10**(6), 673.

15 T. Y. Chang, C. C. Chen, K. M. Cheng, C. Y. Chin, Y. H. Chen, X. A. Chen, J. R. Sun, J. J. Young and T. S. Chiueh, Trimethyl chitosan-capped silver nanoparticles with positive surface charge: their catalytic activity and antibacterial spectrum including multidrug-resistant strains of Acinetobacter baumannii, *Colloids Surf., B*, 2017, **155**, 61–70.

16 A. J. Choudhury, D. Gogoi, R. Kandimalla, S. Kalita, Y. B. Chaudhari, M. R. Khan, J. Kotoky and J. Chutia, Penicillin impregnation on oxygen plasma surface functionalized chitosan/Antheraea assama silk fibroin:

Open Access Article. Published on 02 June 2020. Downloaded on 1/17/2026 12:49:57 PM. This article is licensed under a Creative Commons Attribution-NonCommercial 3.0 Unported Licence.

studies of antibacterial activity and antithrombogenic property, *Mater. Sci. Eng., C*, 2016, **60**, 475–484.

17 J. H. Kim, N. H. Kim, E. J. Kim, J. Kim, M. Y. Lee, Y. H. Park, J. Lee, S. C. Park and M. K. Jang, Antibacterial effects of amino acids-grafted water-soluble chitosan against drug-resistant bacteria, *Biotechnol. Bioprocess Eng.*, 2016, **21**, 183–189.

18 B. P. Antunes, A. F. Moreira, V. M. Gaspar and I. J. Correia, Chitosan/arginine-chitosan polymer blends for assembly of nanofibrous membranes for wound regeneration, *Carbohydr. Polym.*, 2015, **130**, 104–112.

19 X. Zhang, Y. J. Duan, D. F. Wang and F. L. Bian, Preparation of arginine modified PEI-conjugated chitosan copolymer for DNA delivery, *Carbohydr. Polym.*, 2015, **122**, 53–59.

20 X. Hu, A. Ahmeda and M. M. Zangeneh, Chemical characterization and evaluation of antimicrobial and cutaneous wound healing potentials of gold nanoparticles using Allium saralicum RM Fritsch, *Appl. Organomet. Chem.*, 2020, **34**(4), e5484.

21 S. Kumar, R. K. Majhi, A. Singh, M. Mishra, A. Tiwari, S. Chawla, P. Guha, B. Satpati, H. Mohapatra, L. Goswami, *et al.*, Carbohydrate-Coated Gold-Silver Nanoparticles for Efficient Elimination of Multidrug Resistant Bacteria and *In Vivo* Wound Healing, *ACS Appl. Mater. Interfaces*, 2019, **11**, 42998–43017.

22 S. S. I. Abdalla, H. Katas, F. Azmi and M. F. M. Busra, Antibacterial and Anti-Biofilm Biosynthesised Silver and Gold Nanoparticles for Medical Applications: Mechanism of Action, Toxicity and Current Status, *Curr. Drug Delivery*, 2020, **17**, 88–100.

23 M. A. P. Yoosaf, A. Jayaprakash, S. Ghosh, V. S. Jaswal, K. Singh, S. Mandal, M. Shahid, M. Yadav, S. Das and P. Kumar, Zein film functionalized with gold nanoparticles and the factors affecting its mechanical properties, *RSC Adv.*, 2019, **9**, 25184–25188.

24 X. N. Li, S. M. Robinson, A. Gupta, K. Saha, Z. W. Jiang, D. F. Moyano, A. Sahar, M. A. Riley and V. M. Rotello, Functional Gold Nanoparticles as Potent Antimicrobial Agents against Multi-Drug-Resistant Bacteria, *ACS Nano*, 2014, **8**, 10682–10686.

25 Q. Li, F. Lu, G. F. Zhou, K. Yu, B. T. Lu, Y. Xiao, F. Y. Dai, D. Y. Wu and G. Q. Lan, Silver Inlaid with Gold Nanoparticle/Chitosan Wound Dressing Enhances Antibacterial Activity and Porosity, and Promotes Wound Healing, *Biomacromolecules*, 2017, **18**, 3766–3775.

26 D. You, K. Li, W. L. Guo, G. Q. Zhao and C. Fu, Poly (lactic-*co*-glycolic acid)/graphene oxide composites combined with electrical stimulation in wound healing: preparation and characterization, *Int. J. Nanomed.*, 2019, **14**, 7039–7052.

27 F. Yu, C. H. He, A. Y. Waddad, W. L. L. Munyendo, H. X. Lv, J. P. Zhou and Q. Zhang, N-octyl-N-arginine-chitosan (OACS) micelles for gambogic acid oral delivery: preparation, characterization and its study on *in situ* intestinal perfusion, *Drug Dev. Ind. Pharm.*, 2014, **40**, 774–782.

28 A. Mohandas, S. Deepthi, R. Biswas and R. Jayakumar, Chitosan based metallic nanocomposite scaffolds as antimicrobial wound dressings, *Bioact. Mater.*, 2018, **3**, 267–277.

29 V. Vijayakumar, S. K. Samal, S. Mohanty and S. K. Nayak, Recent advancements in biopolymer and metal nanoparticle-based materials in diabetic wound healing management, *Int. J. Biol. Macromol.*, 2019, **122**, 137–148.

30 Y. Z. Ling, Y. Q. Luo, J. W. Luo, X. Y. Wang and R. C. Sun, Synthesis Optimization of Quaternized Chitosan and its Action as Reducing and Stabilizing Agent for Gold Nanoparticles, *J. Macromol. Sci., Part A: Pure Appl.Chem.*, 2013, **50**, 1194–1200.

31 A. Bourkoula, V. Constantoudis, D. Kontziampasis, P. S. Petrou, S. E. Kakabakos, A. Tserepi and E. Gogolides, Roughness threshold for cell attachment and proliferation on plasma micro-nanotextured polymeric surfaces: the case of primary human skin fibroblasts and mouse immortalized 3T3 fibroblasts, *J. Phys. D: Appl. Phys.*, 2016, **49**, 304002.

32 D. H. Shin, S. Chun, M. W. Ahn, I. H. Song and S. Kim, Effects of cp-Ti Surface Roughness and Directionality on Initial Cell Attachment Behaviors, *Korean J. Met. Mater.*, 2012, **50**, 338–343.

33 L. Weiss, Y. Nessler, M. Novelli, P. Laheurte and T. Grosdidier, On the Use of Functionally Graded Materials to Differentiate the Effects of Surface Severe Plastic Deformation, Roughness and Chemical Composition on Cell Proliferation, *Metals*, 2019, **9**(12), 1344.

34 R. Ogawa, C. Huang, S. Akaishi, H. Sano and H. Hyakusoku, Up-To-Date Knowledge About the Role of Mechanical Forces on Wound Healing, *Wound Repair Regen.*, 2015, **23**, A11.

35 R. Kandra and S. Bajpai, Synthesis, mechanical properties of fluorescent carbon dots loaded nanocomposites chitosan film for wound healing and drug delivery, *Arabian J. Chem.*, 2020, **13**, 4882–4894.

36 S. Morales-Bonilla, C. Torres-Torres, M. Trejo-Valdez, D. Torres-Torres, G. Urriolagoitia-Sosa, L. H. Hernandez-Gomez and G. Urriolagoitia-Calderon, Engineering the optical and mechanical properties exhibited by a titanium dioxide thin film with gold nanoparticles, *Opt. Appl.*, 2013, **43**, 651–661.

37 T. Russo, A. Gloria, R. De Santis, U. D'Amora, G. Balato, A. Vollaro, O. Oliviero, G. Improta, M. Triassi and L. Ambrosio, Preliminary focus on the mechanical and antibacterial activity of a PMMA-based bone cement loaded with gold nanoparticles, *Bioact. Mater.*, 2017, **2**, 156–161.

38 S. Bibi, G. J. Price, T. Yasin and M. Nawaz, Eco-friendly synthesis and catalytic application of chitosan/gold/carbon nanotube nanocomposite films, *RSC Adv.*, 2016, **6**, 60180–60186.

39 S. R. Benhabbour, H. Sheardown and A. Adronov, Cell adhesion and proliferation on hydrophilic dendritically modified surfaces, *Biomaterials*, 2008, **29**, 4177–4186.

40 C. C. Shi, W. J. Yuan, M. Khan, Q. Li, Y. K. Feng, F. L. Yao and W. C. Zhang, Hydrophilic PCU scaffolds prepared by grafting PEGMA and immobilizing gelatin to enhance cell adhesion and proliferation, *Mater. Sci. Eng., C*, 2015, **50**, 201–209.

Open Access Article. Published on 02 June 2020. Downloaded on 1/17/2026 12:49:57 PM.
This article is licensed under a Creative Commons Attribution-NonCommercial 3.0 Unported Licence.

41 L. Y. Yang, Z. Y. Jiang, L. H. Zhou, K. L. Zhao, X. Ma and G. S. Cheng, Hydrophilic cell-derived extracellular matrix as a niche to promote adhesion and differentiation of neural progenitor cells, *RSC Adv.*, 2017, **7**, 45587–45594.

42 S. W. Li, P. P. Bai, Y. Z. Li, C. F. Chen, Y. G. Meng and Y. Tian, Electric Potential-Controlled Interfacial Interaction between Gold and Hydrophilic/Hydrophobic Surfaces in Aqueous Solutions, *J. Phys. Chem. C*, 2018, **122**, 22549–22555.

43 C. T. Wang, W. T. Leung, J. C. Xu, S. C. Fu and C. Y. H. Chao, Droplet detachment behavior from a rough hydrophilic surface, *J. Aerosol Sci.*, 2020, **139**, 105469.

44 M. M. Villar-Chavero, J. C. Dominguez, M. V. Alonso, M. Oliet and F. Rodriguez, Chitosan-reinforced cellulosic bionogels: viscoelastic and antibacterial properties, *Carbohydr. Polym.*, 2020, **229**, 115569.

45 Y. L. Yu, B. L. Tao, J. H. Sun, L. L. Liu and H. Zheng, Fabrication of chitosan-graft-polyaniline-based multilayers on Ti substrates for enhancing antibacterial property and improving osteogenic activity, *Mater. Lett.*, 2020, **268**, 127420.

46 M. Zhaleh, A. Zangeneh, S. Goorani, N. Seydi, M. M. Zangeneh, R. Tahvilian and E. Pirabbasi, *In vitro* and *in vivo* evaluation of cytotoxicity, antioxidant, antibacterial, antifungal, and cutaneous wound healing properties of gold nanoparticles produced *via* a green chemistry synthesis using Gundelia tournefortii L. as a capping and reducing agent, *Appl. Organomet. Chem.*, 2019, **33**(9), e5015.

47 H. J. Yen, Y. A. Young, T. N. Tsai, K. M. Cheng, X. A. Chen, Y. C. Chen, C. C. Chen, J. J. Young and P. D. Hong, Positively charged gold nanoparticles capped with folate quaternary chitosan: synthesis, cytotoxicity, and uptake by cancer cells, *Carbohydr. Polym.*, 2018, **183**, 140–150.

48 H. Hau, D. Khanal, L. Rogers, N. Suchowerska, R. Kumar, S. Sridhar, D. McKenzie and W. Chrzanowski, Dose enhancement and cytotoxicity of gold nanoparticles in colon cancer cells when irradiated with kilo- and mega-voltage radiation, *Bioeng. Transl. Med.*, 2016, **1**, 94–102.

49 R. G. Gourdie and T. A. Myers, *Wound regeneration and repair: methods and protocols*, Springer Science+Business Media, Humana Press, New York, 2013, p. xviii, 585 pages.

50 F. Wittmann, N. Prix, S. Mayr, P. Angele, M. W. Wichmann, N. K. van den Engel, T. Hernandez-Richter, I. H. Chaudry, K. W. Jauch and M. K. Angele, Arginine improves wound healing after trauma-hemorrhage by increasing collagen synthesis, *J. Trauma*, 2005, **59**, 162–168.

51 R. F. de Araujo, A. A. de Araujo, J. B. Pessoa, F. P. F. Neto, G. R. da Silva, A. L. C. S. L. Oliveira, T. G. de Carvalho, H. F. O. Silva, M. Eugenio, C. Sant'Anna, *et al.*, Anti-inflammatory, analgesic and anti-tumor properties of gold nanoparticles, *Pharmacol. Rep.*, 2017, **69**, 119–129.

52 H. Kocic, I. Arsic, M. Stankovic, D. Tiodorovic, V. Ciric and G. Kocic, Proliferative, Anti-Apoptotic and Immune-Enhancing Effects of L-Arginine in Culture of Skin Fibroblasts, *J. Biol. Regul. Homeostatic Agents*, 2017, **31**, 667–672.

53 Y. Zhu, C. Yu and S. G. Zhuang, Protein arginine methyltransferase 1 mediates renal fibroblast activation and fibrogenesis through activation of Smad3 signaling, *American Journal of Physiology-Renal Physiology*, 2020, **318**, F375–F387.